Wind Energy

WIND ENERGY
Wind Energ. 2016; **19**:151–166
Published online 19 February 2015 in Wiley Online Library (wileyonlinelibrary.com). DOI: 10.1002/we.1828

RESEARCH ARTICLE

Analysis of throw distances of detached objects from horizontal-axis wind turbines

Hamid Sarlak and Jens N. Sørensen

Section of Fluid Mechanics, Department of Wind Energy, Technical University of Denmark, DK-2800 Lyngby, Denmark

ABSTRACT

This paper aims at predicting trajectories of the detached fragments from wind turbines, in order to better quantify consequences of wind turbine failures. The trajectories of thrown objects are attained using the solution to equations of motion and rotation, with the external loads and moments obtained using blade element approach. We have extended an earlier work by taking into account dynamic stall and wind variations due to shear, and investigated different scenarios of throw including throw of the entire or a part of blade, as well as throw of accumulated ice on the blade. Trajectories are simulated for modern wind turbines ranging in size from 2 to 20 MW using upscaling laws. Extensive parametric analyses are performed against initial release angle, tip speed ratio, detachment geometry, and blade pitch setting. It is found that, while at tip speeds of about 70 m/s (normal operating conditions), pieces of blade (with weights in the range of approximately 7-16 ton) would be thrown out less than 700 m for the entire range of wind turbines, and turbines operating at the extreme tip speed of 150 m/s may be subject to blade throw of up to 2 km from the turbine. For the ice throw cases, maximum distances of approximately 100 and 600 m are obtained for standstill and normal operating conditions of the wind turbine, respectively, with the ice pieces weighting from 0.4 to 6.5 kg. The simulations can be useful for revision of wind turbine setback standards, especially when combined with risk assessment studies.

KEYWORDS
wind turbine accidents; blade element theory; blade detachment; ice throw; aerodynamic model; HAWT

Correspondence
H. Sarlak, Section of Fluid Mechanics, Department of Wind Energy, Technical University of Denmark, DK-2800 Lyngby, Denmark.
E-mail: hsar@dtu.dk

Received 6 May 2014; Revised 18 December 2014; Accepted 21 December 2014

1. INTRODUCTION

The ever-growing number of wind turbines installed near inhabited areas, buildings and community facilities, such as bridges, power installations or highways, has resulted in an increasing concern by authorities to determine risk levels associated with wind turbine blade failure. From a safety point of view, the most serious failure is associated with splintering of rotor blades and detachment of debris, which could be thrown over long distances and damage people or property. Ice-throw from wind turbines installed in cold climate is also of high concern, especially for wind turbines erected near highways where the ice pieces thrown from a wind turbine may strike a passing car, which in the worst case may cause a fatal accident.

Various types of hazards regarding operation of wind turbines have recently been reported by Durstwitz and the Caithness Windfarm Information Forum.[2,3] According to a recent survey by the Caithness Windfarm Information Forum, blade failures resulting in either whole blades or pieces of blades being thrown from the turbine are the most important causes of turbine accidents.[3] A comparative graph showing the growth of wind turbine accidents over the past four decades is shown in Figure 1, where the share of blade accidents and accidents due to fire, which may eventually cause throw of fire patches, are also presented. Due to such accident data, energy authorities all over the world have tried to enforce safety distances around wind turbines and wind farms. The safety distance is a distance within which it is not allowed to build human structures such as buildings and roads. Shown in Table I is an example of the safety distance standards defined by different authorities. It can be seen from the table the values of offset safety distances fall within an extensive range of

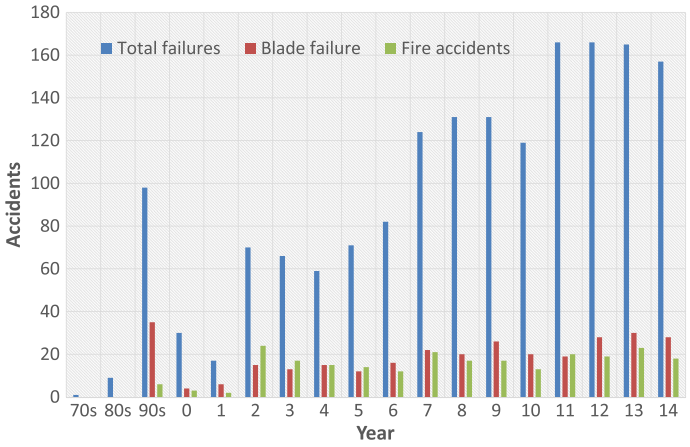

Figure 1. Comparison of wind turbine accidents and particularly blade failure data in a period from 1970s until 2014 (data taken from Caithness Windfarms[3]).

Table I. Safety distances of wind turbines from human structures as practiced in different regions of the world.[17]

Authority/source	Safety distance [m] (ft)
France	1609 (5280)
Germany	1609 (5280)
Rural Manitoba, Canada (1981)	(6500)
US National Research Council	762 (2500)
IL, USA	457 (1500)
Riverside County, CA, USA	**3218 (10560)**
MI, USA	**304 (1000)**

scales between 3.2km and 300m, and that the setback standards are not even similar in different regions of the same country. To standardize such safety guidelines, it is useful to employ mathematical models of the throw in various conditions and risk assessment tools to associate the probability of failure in each particular setting.

Motions of solid particles in fluids were first addressed analytically by Kirchhoff.[4] He showed that the equations of motion for a solid body in an ideal fluid reduce to a set of ordinary differential equations (ODE) based on Euler's equations. Further experimental investigations on falling objects revealed, despite originating from Euler's equations, various states of chaotic motion. It was also mathematically shown that Kirchhoff's equations had been prone to yield chaotic solutions [5]. Tanabe *et al.*[6] developed a set of two-dimensional equations of motion (including rotation) based on simple mechanics in which plates of zero thickness were subject to lift, friction and gravity forces. Based on those assumptions, they found five different falling patterns, ranging from a periodic movement to chaotic random motions depending on the density ratio between the solid and the surrounding fluid and on the length of the object. Pesavento and Wang[7] and Andersen *et al.*[8] performed more detailed studies to determine the motion of a falling two-dimensional elliptic object using direct numerical simulation of the Navier–Stokes equations. They took added mass and added moment of inertia into account and analyzed the transient motion and local jumps of the falling object thoroughly.

Due to complications in a real-life blade accidents (erratic motions, high Reynolds numbers, complex geometries etc.), the fundamental studies mentioned above could only partially help understanding the physics of wind turbine blade throw patterns. To cope with the wind turbine problems, simplified approaches were used. Macqueen *et al.*,[9] for instance, studied the problem of blade-throw from wind turbines, using classical ballistics and also assumption of constant lift and drag. A lift coefficient of Cl = 0.8 and a drag coefficient of Cd = 0.4 were used for the gliding simulations, with Cl = 0.0 and Cd = 1.0 for the tumbling motion. However, the probability that gliding would occur was deemed very small. Their maximum throw studies using simple ballistic analysis, that is, by neglecting aerodynamic forces, showed that in the extreme throw velocity of approximately 310m/s, the maximum throw length reaches 10km.

One of the first detailed studies on the aerodynamics of a detached wind turbine blade was performed by Sørensen[1] using a blade element approach. In this approach, the detached blade is divided into a number of sections and the aerodynamic loads are determined for each section. The total external aerodynamic load on the whole blade would then be determined as the summation of the individual forces on each section.

Wind Energ. 2016; **19**:151–166 © 2015 John Wiley & Sons, Ltd.
DOI: 10.1002/we

Recently, Rogers *et al.*[10] used a dynamic model employing quaternions instead of Euler angles and rotation vectors to form the orientation matrix and performed Monte Carlo simulations of a large set of initial conditions in order to obtain a range of the throw distances.

Ice throw has also been investigated, especially for the turbines erected in the cold climate. Seifert *et al.* measured ice-throw accidents together with a simple aerodynamic model and performed risk analysis of the ice fragments thrown from the blades.[11] Recently, a model of ice throw for a wind turbine in operation was presented by Biswas *et al.*,[12] in which calculations were carried out for ice pieces by neglecting lift and using a fixed drag coefficient of $C_d = 1.0$. It was also estimated that including the highest possible, lift increases the throw distance by approximately a factor of two.

The problem of blade/ice throw has also been investigated through the window of probabilistic methods. Such methods deal with risk levels and probabilities that a certain throw distance will occur. Such studies are typically performed together with a dynamic model for calculating the throw distances. Macqueen *et al.*,[9] Morgan,[13] Morgan and Bossanyi[14] and Rogers *et al.*[10] carried out risk analyses of ice throw to determine safety guidelines for wind developments in ice-prone areas. Sørensen[15] proposed a statistical model that determines risk levels of debris hitting people. Similarly, Carbone and Afferrante[16] performed a combined probabilistic and dynamic analyses to quantify hazards due to the blade throw.

In the present work, detailed aerodynamic analysis are performed for simulating flying debris. The cases include blade throw in which the blade together with its components is thrown, a case in which only a shell laminate is thrown and a case involving detachment of ice fragments. The governing equations of motion form a set of 18 ODEs responsible for the six degree-of-freedom motion. The resulting system of discretized equations are solved using an ordinary time integration method. Throw distances for four different turbine sizes ranging from 2.3 to 20 MW are compared, by employing simple upscaling rules. The computations are carried out for different wind and tip speeds.

2. MATHEMATICAL MODELING

The equations of motion for a detached blade include equations of translation and equations of rotation. These are obtained using Newton's second law and Euler's equations of motion, with the aerodynamic forces obtained from tabulated airfoil data. To be able to quantify the rotational motion of the detached blade, the moments of inertia around the rotation axes are calculated. This, however, cannot be calculated in a fixed coordinate system (i.e., an inertial system) since both the moments of inertia and the rotational speeds are varying and a solution would become very complicated. Instead, the equations are computed around the body-fixed principal axis, and the obtained values are subsequently transformed to the global (inertial) coordinate system to represent the absolute location and orientations. Two coordinate systems are defined here: a global coordinate system $\mathbf{x} = (x, y, z)$ with the origin on the tower basement and orthonormal right-handed unit vectors $(\vec{i}, \vec{j}, \vec{k})$, with the y-axis in the wind direction and the z-axis in the upward direction. A body-fixed coordinate system $\mathbf{b} = (x_b, y_b, z_b)$ is defined by an orthonormal right-handed unit vector $(\vec{r}_1, \vec{r}_2, \vec{r}_3)$, with the origin located at the center of gravity of the detached blade fragment and the third axis parallel to the length axis of the blade (Figure 2).

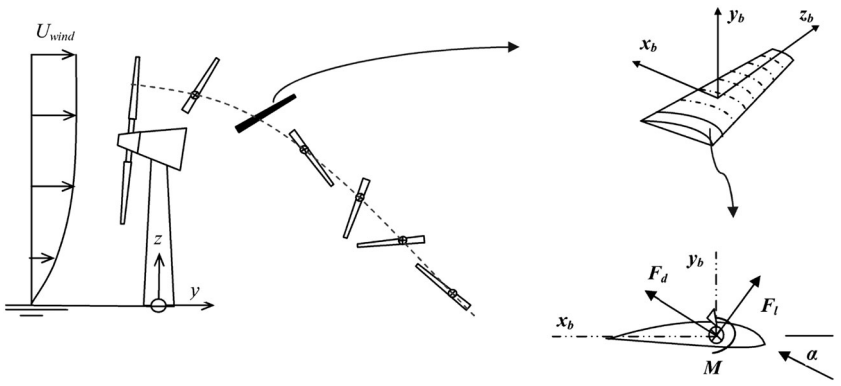

Figure 2. Sketch of the problem and definition of coordinate systems.

The orientation of the detached part is determined through a matrix **R**, which gives the transformation from global coordinates to the body-fixed coordinates

$$\begin{bmatrix}\vec{r}_1\\ \vec{r}_2\\ \vec{r}_3\end{bmatrix} = \left[\mathbf{R}\right]\begin{bmatrix}\vec{i}\\ \vec{j}\\ \vec{k}\end{bmatrix} = \begin{bmatrix}r_{11} & r_{12} & r_{13}\\ r_{21} & r_{22} & r_{23}\\ r_{31} & r_{32} & r_{33}\end{bmatrix}\begin{bmatrix}\vec{i}\\ \vec{j}\\ \vec{k}\end{bmatrix} \quad \text{and similarly,} \quad \begin{bmatrix}\vec{i}\\ \vec{j}\\ \vec{k}\end{bmatrix} = \left[\mathbf{R}^{-1}\right]\begin{bmatrix}\vec{r}_1\\ \vec{r}_2\\ \vec{r}_3\end{bmatrix} \tag{1}$$

Equation (1) holds for transformation of any variable between the two coordinate systems. This way of defining a vectorized rotation matrix (as opposed to Euler's scalar angles) ensures uniqueness of orientation angles and avoids the problem known as gimbal lock.

The full six degree-of-freedom motion is governed by Newton's second law of motion and Euler's equations of motion:

$$m\underline{\ddot{x}}_g = \underline{F} + m\underline{g} \tag{2}$$

$$\underline{\underline{I}}.\underline{\dot{\omega}}_b = \underline{\omega}_b \times (\underline{\underline{I}}.\underline{\omega}_b) = \underline{M} \tag{3}$$

where m is the mass of the blade, $\underline{x}_g$ is the position vector of the center of gravity, $\underline{F}$ is the aerodynamic force acting on the center of gravity, g is the gravitational acceleration, $\underline{\underline{I}}$ is the moment of inertia tensor, $\underline{\omega}$ is the angular velocity in the rotating frame of reference, $\underline{M}$ is the aerodynamic force acting along the principal axis of the moment of inertia tensor and (.) denotes differentiation with respect to time. To close the system, the following relationship between the motion of the unit vectors of the body (the blade fragment) and the angular velocity is used:

$$\dot{\underline{r}} = \underline{\omega} \times \underline{r} \tag{4}$$

where $\underline{\omega}$ is the angular velocity of the blade fragment in the inertial coordinate system, which by equation (1) is transformed into the local body-fixed coordinate system. The total set of equations are solved using a fourth-order Runge–Kutta–Nystrom or a third-order Adams–Bashforth method. For more information about the mathematical and numerical treatment of the equations, readers are referred to the early work of Sørensen.[1]

2.1. Aerodynamic modeling

For the solution of the system of ODEs, a blade element approach is employed in which each blade is divided into n sections along the span. In each section, the external forces and moments are calculated from airfoil data based on the local wind speed and relative velocities.

The three-dimensional edge effects are to some extent considered through the finite aspect ratio assumption of the blade, and the aerodynamic coefficients of lift and drag are calculated for all angles of attack based on flat-plate theory. The induced velocities are, however, neglected, and the Reynolds-number dependence of the airfoil data is disregarded. Once the aerodynamic coefficients are found, the lift, drag and moments on the blade fragment are computed as

$$L_i = \frac{1}{2}\rho v_i^2 A_i C_{Li}, \quad D_i = \frac{1}{2}\rho v_i^2 A_i C_{Di} \tag{5}$$

where L_i and D_i are lift and drag forces on the i-th section, ρ is the air density, v_i is the local relative airspeed, $A_i = c_i \Delta r_i$ is the local planform area where c_i and Δr_i are the local chord and the section lengths, and C_{Li} and C_{Di} are the sectional lift and drag coefficients at the desired angle of attack.

The static forces aerodynamic coefficients of the airfoil only depend on the angle of attack. Unsteady effects at high angles of attack are included by using the dynamic stall model of Øye.[18] In this model, the dynamic lift coefficient is obtained by interpolating between the lift coefficient of an airfoil in a fully attached flow and a lift coefficient of the airfoil when the flow around the airfoil is fully separated, i.e.,

$$C_{l,dyn} = f_s C_{l,inv}(\alpha) + (1 - f_s) C_{l,fs}(\alpha) \tag{6}$$

where $C_{l,inv}$ is the lift coefficient for a fully attached flow (i.e., inviscid flow assumption) and $C_{l,fs}$ is the lift coefficient for fully separated flow. The stall-changing rate is defined as

$$\frac{df_s}{dt} = \frac{f_s^{st} - f_s}{\tau} \tag{7}$$

where f_s is the time-dependent separation function, which can be thought of as the unsteady weighting function between the fully attached and the fully separated flow. f_s^{st} is a function of airfoil section,

$$f_s^{st}(\alpha) = \frac{C_{l,st}(\alpha) - C_{l,fs}(\alpha)}{C_{l,inv}(\alpha) - C_{l,fs}(\alpha)} \tag{8}$$

Wind Energ. 2016; **19**:151–166 © 2015 John Wiley & Sons, Ltd.
DOI: 10.1002/we

and τ is an empirically determined time constant giving the time lag between the dynamic value of f_s and its static value. It follows from equation (7) that

$$f_s(t+\Delta t) = f_s^{st} + \left(f_s(t) - f_s^{st}\right)\exp\left(\frac{-\Delta t}{\tau}\right) \tag{9}$$

2.2. The atmospheric boundary layer effects

The inlet wind is included as a velocity profile corresponding to the Atmospheric Boundary Layer (ABL). As a result, in addition to simulating uniform inflow,[1] it is possible to simulate throw distances for blades thrown in wind fields following a power or logarithmic law, depending on the specific site information. The ABL wind profile as a function of height and atmospheric conditions reads

$$u_z = \frac{u_*}{\kappa}\left[\ln\left(\frac{z}{z_0}\right) + \psi(z, z_0, L)\right] \tag{10}$$

where u_* is the friction velocity, κ is the von Karman constant (~ 0.41), z_0 is the roughness length, ψ is a function of atmospheric stability and L is the Monin–Obukhov stability parameter (see Wyngaard[19] for more details).

If no data are available in a specific site, and neutral ABL is assumed, a power law $u(z) = u_{hub}(z/z_{hub})^{\alpha}$, $\alpha \sim 0.14$ will be used for the wind velocity at different heights having the wind velocity at hub height as an input. The power-law method is used for the parametric studies in this paper.

Using the mentioned wind profile and denoting the local position vector of a point p on the wing as $\vec{r}_{pb}$, the local relative wind velocity $\vec{u}_{pb}$, as seen by the blade fragment, is given as

$$\vec{u}_{pb} = \left[\mathbf{R}\right].(\vec{u}_{wind} - \vec{u}_g) - \vec{\omega}_b \times \vec{r}_{pb} \tag{11}$$

where the wind vector is assumed to be $\vec{u}_{wind} = (0, u_y, 0)$, neglecting the vertical and lateral components.

3. SIMULATION RESULTS

Simulations of both blade-throw and ice-throw distances are performed by solving the equations derived in the previous sections using the in-house aerodynamic code *Savbal*[*]. The overall procedure for the solution consists of three stages, comprising coordinate transformation, aerodynamics load assessment and time integration. The initial position, orientation and velocities of the detached part are first evaluated at their local coordinates. Based on these values, an iterative procedure starts where the local velocities are evaluated, according to exerted aerodynamic loads, and integrated to give the location and orientation of the fragment in global coordinates until the fragment reaches the ground level.

For the blade-throw analysis, cases with different detached lengths and tip speeds are compared in two sub-cases: (1) the whole blade together with its sandwich structure is thrown and (2) only the shell layer of the blade is thrown. For ice-throw analysis, it turns out that the drag to mass ratio plays an important role for the magnitude of the throw distance. As a result, a few cases with different C_dA/m ratios (as discussed by Biswas *et al.*[12]) with both standstill and running turbine conditions are simulated. The analyses are performed for different wind turbine sizes.

3.1. Turbine upscaling laws

The throw distance analysis was initially performed for a 2.3 MW turbine using publicly available data. A series of empirical relations was then used to upscale the data for the larger turbines, and the analyses were performed for four different wind turbine sizes, i.e., 2.3, 5, 10 and 20 MW. The scale-up factors are first obtained for the blade length, which scales as the square root of the power ratio. Therefore, denoting the blade length, mass (applicable to both total sandwich structure and the shell laminate masses) and mass moment of inertia for the reference turbine with index a, i.e., r_a, m_a and $\mathbf{I_a}$, respectively, the corresponding values for the upscaled turbine, index b, can be obtained as

$$r_b = r_a\left(\frac{P_b}{P_a}\right)^{S_l},\quad m_b = m_a\left(\frac{r_b}{r_a}\right)^{S_m},\quad \mathbf{I}_b = \mathbf{I}_a\left(\frac{m_b}{m_a}\right)\left(\frac{r_b}{r_a}\right)^2 = \mathbf{I}_a\left(\frac{r_b}{r_a}\right)^{S_m+2} \tag{12}$$

[*]The computing code *Savbal* will be available upon request for further studies on this field.

Table II. Characteristics of different turbine sizes considered in the throw analyses.

Size	$L^* = \frac{L}{R}$	L (m)	m (kg)	I_x (kg·m^2)	I_y (kg·m^2)	I_z (kg·m^2)
2.3 MW $R = 45$ m, $H = 100$ m	1.0	45	7.3E+3	0.1E+7	0.1E+7	0.3E+04
	0.5	22.5	2.4E+3	0.1E+6	0.1E+6	0.40E+03
	0.2	10	4.1E+2	0.4E+04	0.4E+04	0.2E+02
5 MW $R = 66$ m, $H = 147$ m	1.0	66	2.6E+04	0.9E+07	0.9E+07	0.2E+05
	0.5	33	8.2E+03	0.1E+07	0.1E+07	0.3E+04
	0.2	14	1.7E+3	0.3E+05	0.3E+05	0.2E+03
10 MW $R = 93$ m, $H = 208$ m	1.0	93	8.2E+04	0.5E+08	0.5E+08	0.1E+06
	0.5	46.5	2.7E+04	0.6E+07	0.6E+07	0.2E+05
	0.2	20	5.3E+3	0.2E+06	0.2E+06	0.1E+04
20 MW $R = 132$ m, $H = 294$ m	1.0	132	2.6E+05	0.3E+09	0.3E+09	0.9E+06
	0.5	66	8.7E+04	0.4E+08	0.4E+08	0.1E+06
	0.2	29	1.6E+04	0.1E+07	0.1E+07	0.8E+04

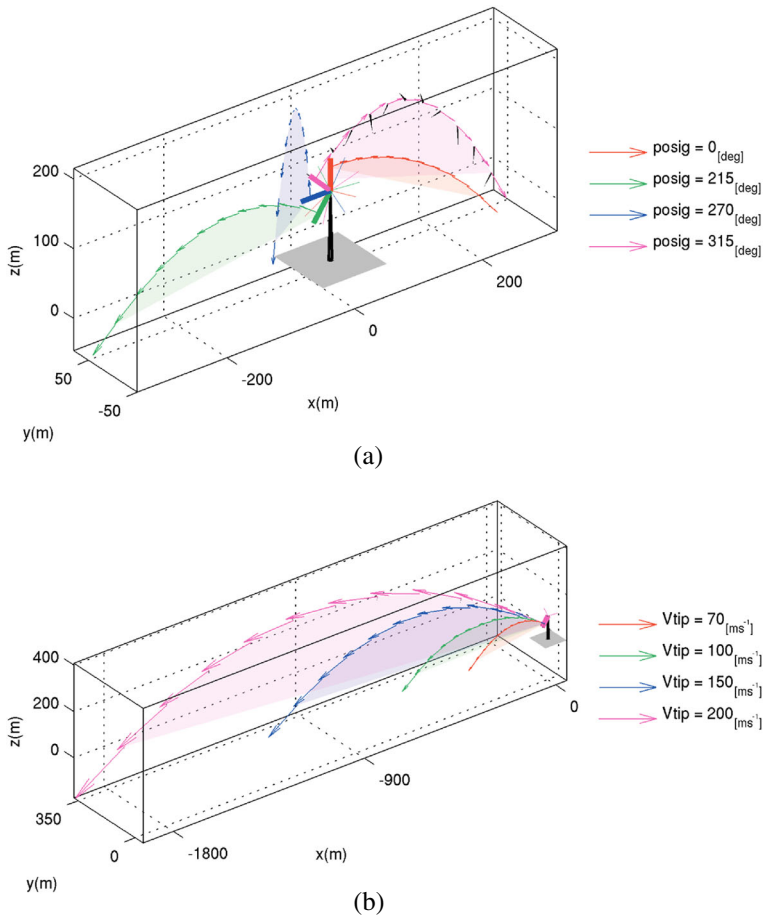

Figure 3. Schematic graphs of the throw distances for half-blade detachment changing (a) the initial release angles (upward-clockwise reference) and (b) the tip speed velocities for the 2.3 MW reference turbine.

where $\mathbf{I} = (I_x, I_y, I_z)$. In the previous relations, $S_l = 1/2$ and S_m depends on actual scaling laws when increasing the size of the rotor. From simple upscaling rules, S_m would be equal to 3 , but because of more elaborate rotor designs, this parameter is usually found to be somewhat smaller. In the present work, we employ $S_m = 2.3$ (see UpWind[20] and TPI Composites[21] for more information on turbine scaling).

Wind Energ. 2016; **19**:151–166 © 2015 John Wiley & Sons, Ltd.
DOI: 10.1002/we

3.2. Full-blade throw analysis

In this section, the throw distance analyses are performed for four different turbine sizes based on the upscaling rules presented previously. Here, the term full blade refers to the case of blade shell including stiffening members (upper and lower shells, spar, etc.). The dimensions and other characteristics of each turbine size are reported in Table II. In accordance with the copyright policies of the turbine manufacturers, the data for the reference turbine (2.3 MW) do not correspond to an existing turbine but are chosen to mimic a real turbine.

The analysis included a parametric study, where the effects of the length of the detached parts, incoming wind speeds, blade tip speeds and wind turbine size on the blade-throw distances were investigated. The height of the tower is in all considered cases assumed to be equal to the rotor diameter. Figure 3 shows three-dimensional visualizations of the throw distances of a half-blade piece thrown of the 2.3 MW machine for different initial conditions. The small colored patches in the figure shows the instantaneous orientation of the detached part. For the sake of clarity, only some selected curves are shown in the figure. Figure 3(a) shows the effect of release angle on the throw distance, and Figure 3(b) shows the effect

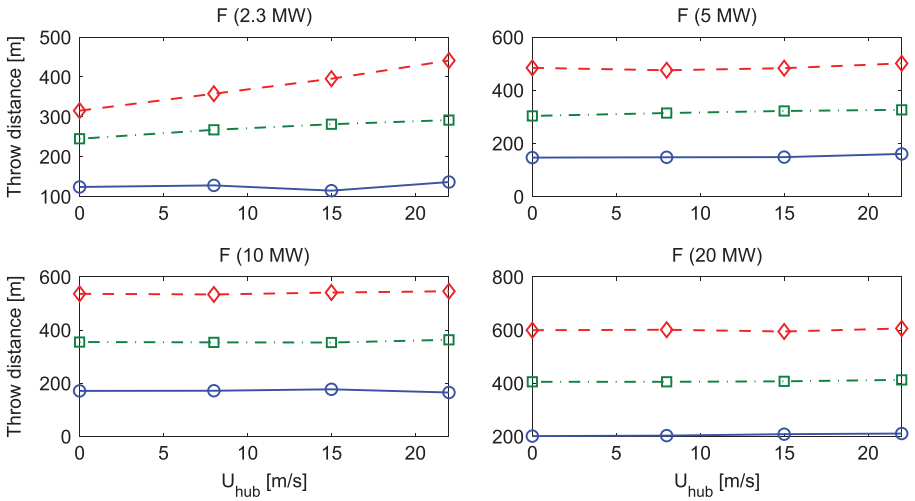

Figure 4. Throw distance calculations of full blade with three different detached lengths for 2.3, 5, 10 and 20 MW turbines at the normal operating condition of $V_{tip} = 70$ m/s. The horizontal axis shows the wind speed at the hub height and the vertical axis represents the throw distance. ◇ ◇ ◇: $L^* = 0.2$; □ □ □: $L^* = 0.5$; and o o o: $L^* = 1$.

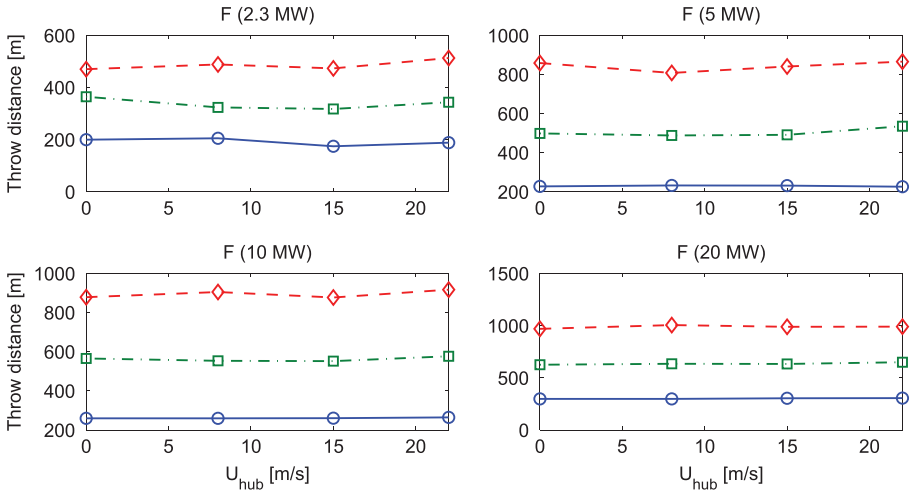

Figure 5. Throw distance calculations of full blade with three different detached lengths at a high tip speed of $V_{tip} = 100$ m/s. Legends are similar to those in Figure 4.

of release tip velocity. As can be seen, the release tip speed is a very important factor influencing the maximum throw distances. Normal operating conditions with $V_{tip} = 70$ m/s result in throw distances of about 500 m long, whereas a tip speed of $V_{tip} = 150$ m/s may lead to throw distances up to 2 km.

For the quantitative analysis performed in the next section, the fragments are thrown at a release angle of 45° from the horizon (225° measured upward-clockwise) in all calculations. The full-blade and blade-shell throw calculations are performed using flat-plate assumption for the aerodynamic coefficients.

Figures 4, 5 and 6 show the throw distances for three different fragments of the full blade for a combination of three blade tip speeds ($v_{tip} = 70,\ 100\ 150$ m/s) and four different incoming wind velocities (with power-law profiles) ranging between 0 and 22 m/s at hub height.

The figures are divided into three groups, the first group (Figure 4) shows the throw distances, relative to the tower position, for different incoming wind speeds (shown on the horizontal axis) and different detachment lengths at a tip speed of $V_{tip} = 70$ m/s. The detachment length L^*, shown with markers, is the length of the detached piece, measured from the blade tip and normalized by the blade length. The throw distances are calculated and plotted for the four considered wind turbine sizes ranging from 2.3 to 20 MW. As can be seen, except for the 2.3 MW machine, the effect of the incoming wind on the throw distance is almost negligible. Similarly, the effect of turbine size on the throw distance is minimal and the main

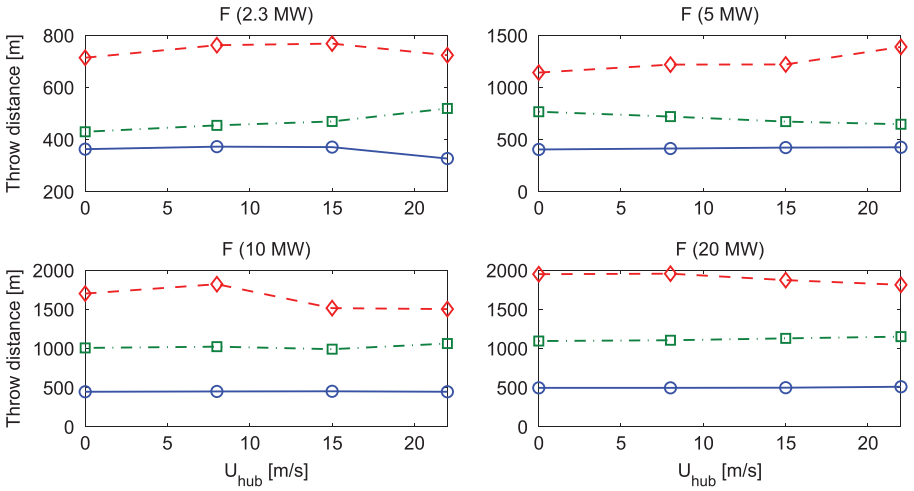

Figure 6. Throw distance calculations of full blade with three different detached lengths at an extreme tip speed of $V_{tip} = 150$ m/s. Legends are similar to those in Figure 4.

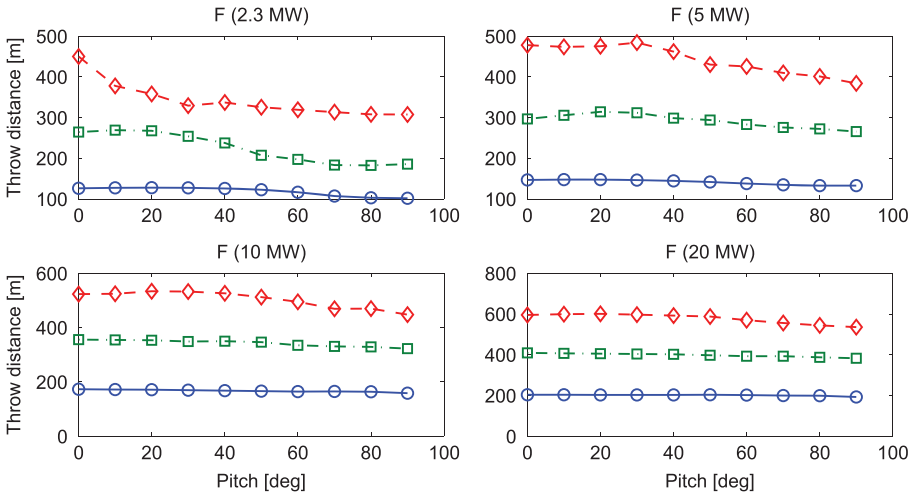

Figure 7. Sensitivity of throw distances of full blade to the initial pitch setting for 2.3, 5, 10 and 20 MW turbines operating at $V_{tip} = 70$ m/s. ◇ ◇ ◇: $L^* = 0.2$; □ □ □: $L^* = 0.5$; and o o o: $L^* = 1$.

Wind Energ. 2016; **19**:151–166 © 2015 John Wiley & Sons, Ltd.
DOI: 10.1002/we

parameter governing the throw distance is the detachment length. The minimum throw distance is obtained for the heaviest fragment ($L^* = 0.2$) thrown from the 2.3 MW turbine, while the maximum throw distance of all cases at $V_{tip} = 70$ m/s is around 600 m for the lightest fragment ($L^* = 0.2$).

Figure 5 shows the same graphs for the higher tip speed of $V_{tip} = 100$ m/s, where the maximum throw distances for the smallest and largest turbines are about 500 and 1000 m, respectively, while the minimum throw distance is reached for a full-blade throw ($L^* = 1$) of a 2.3 MW turbine. Also, it is clear that the effect of the hub-height wind velocity is still very small. Figure 6 shows the same plots for the most extreme case considered, i.e., using a tip speed of $V_{tip} = 150$ m/s. Here, the thrown pieces reach throw distances ranging from approximately 350 m for the full-blade throw for a 2.3 MW turbine to about 2000 m for the lightest fragment thrown from the 20 MW turbine.

As can be seen from the red curve in Figure 6 for the 10 MW turbine (bottom-left), the throw distance has unexpectedly decreased when increasing the wind speed from 10 to 15 m/s. This behavior is somehow repeated to a smaller extent in other cases, especially at higher tip velocities. The unexpected results can happen because of the fact that a small change in the initial conditions can change the force/moment distributions on the fragments, thereby changing the trajectory drastically. To investigate the erratic motion further, the effect of initial pitch setting on the trajectory is analyzed in the next section.

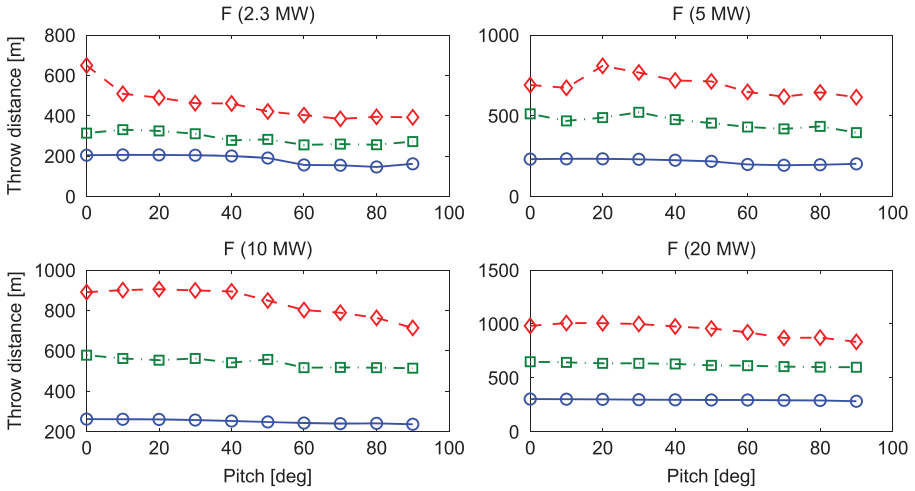

Figure 8. Sensitivity of throw distances of full blade to the initial pitch setting at $V_{tip} = 100$ m/s. Legends are similar to those in Figure 7.

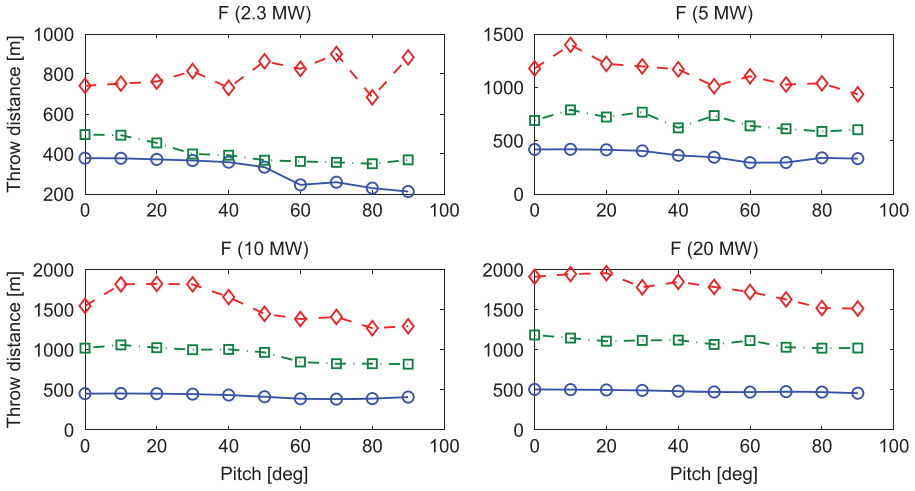

Figure 9. Sensitivity of throw distances of full blade to the initial pitch setting at $V_{tip} = 150$ m/s. Legends are similar to those in Figure 7.

3.2.1. Effect of initial pitch settings.

As explained earlier, analyses of the throw trajectories show that the throw distance for a particular wind turbine sometimes exhibits an erratic behavior going from one dominant solution to another with only a slight change in the initial conditions.

Table III. Aspect ratios, reference chord length C_{ref} and detached mass m of the blade shells ($\rho_{shell} = 1700$ kg/m^3) used for throw simulation from turbines of different sizes.

	2.3 MW		5 MW		10 MW		20 MW	
Cases − AR	C_{ref} (m)	m (kg)	C_{ref} (m)	m (kg)	C_{ref} (m)	m (kg)	C_{ref} (m)	m (kg)
$AR = 1$		34		83		184		408
$AR = 5$	1	170	1.5	415	2.1	920	3	2040
$AR = 10$		340		830		1840		4080

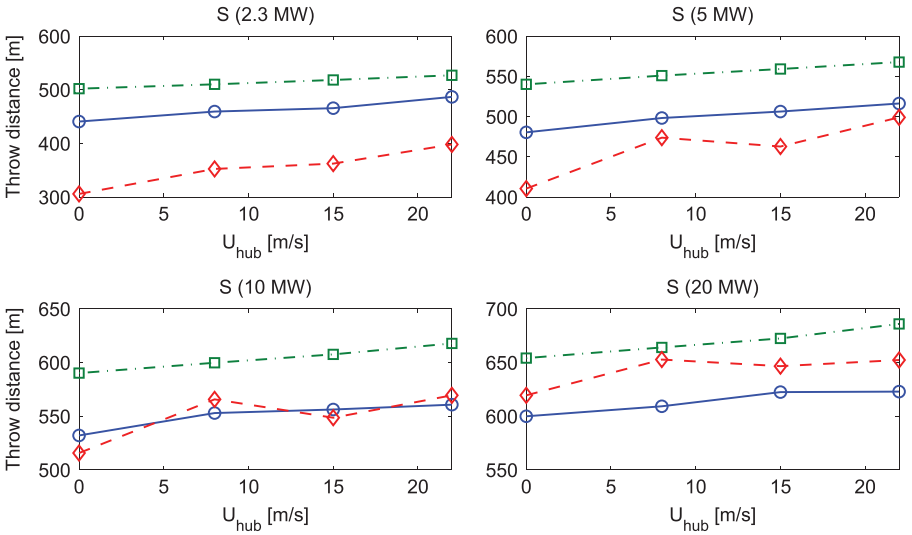

Figure 10. Throw distance calculations of blade shell with three different aspect ratios (invariant chord length for each turbine) for 2.3, 5, 10 and 20 MW turbines at a normal operating condition of $V_{tip} = 70$ m/s. ◇ ◇ ◇: $AR = 1$; □ □ □: $AR = 5$; and o o o: $AR = 10$.

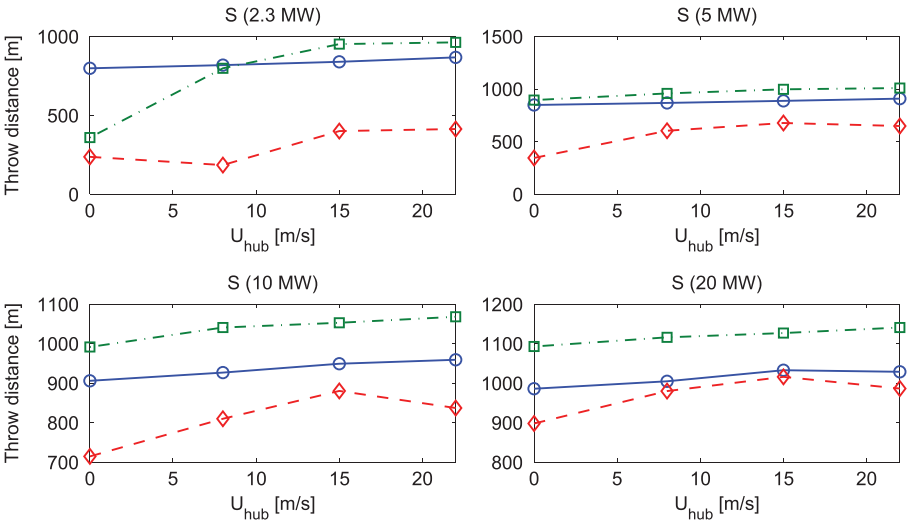

Figure 11. Throw distance calculations of blade shell at high tip speed of $V_{tip} = 100$ m/s. Legends are similar to those in Figure 10.

Wind Energ. 2016; **19**:151–166 © 2015 John Wiley & Sons, Ltd.
DOI: 10.1002/we

To understand this behavior, a sensitivity study is performed to investigate the effects of the initial pitch settings on the trajectory. Figures 7–9 demonstrate the pitch angle dependence of the full-blade throw distances for different turbine sizes and tip speeds, where the throw distances are obtained for release pitch angles ranging from 0° to 90°. As can be seen, the pitch setting has a substantial impact especially for the lighter parts. In general, higher throw distances are achieved using fragments thrown at lower pitch angles, which are due to the reduced drag. The effect of pitch angle on the heavier pieces (green and blue curves) is, however, smaller. The reason for this is that the aerodynamics plays a less significant role for the heavy parts in the throw distance calculation and the distance is mainly governed by the inertial forces. For the extreme tip velocity, and especially for the 2.3 MW turbine, increasing the pitch angle produces erratic throw distances for the lightest fragments. The exact reason for such erratic behavior has not been yet understood, but it is most likely explained by the physics of the problem, as explained earlier.

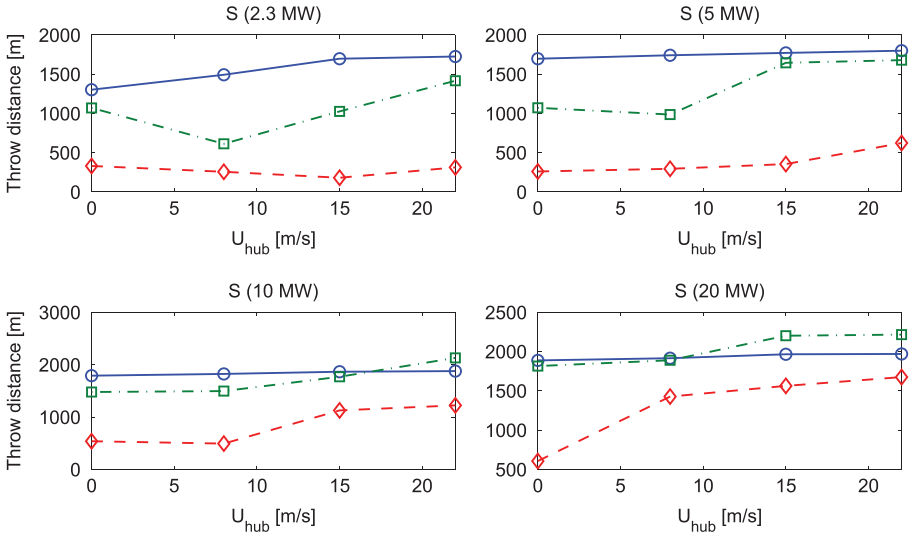

Figure 12. Throw distance calculations of blade shell at an extreme tip speed of V_{tip} = 150 m/s. Legends are similar to those in Figure 10.

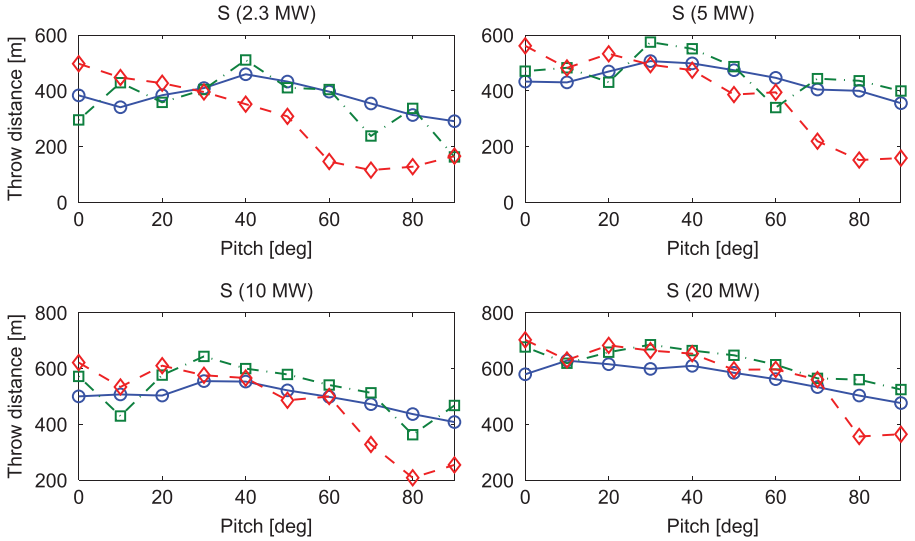

Figure 13. Sensitivity of throw distances of blade shell to the initial pitch setting at V_{tip} = 70 m/s. Legends are the same as in Figure 10.

3.3. Blade-shell throw analysis

An analysis of available data from blade failure accidents shows that depending on the manufacturing method and the structural integrity of the blade, it might first shatter into lighter parts, with the consequence that the shell layer is most likely to be thrown away. Three cases of different aspect ratios are considered for the shell throw analyses. For the reference case of 2.3 MW turbine, an average chord of 1 m and a shell thickness of 2 cm are chosen, and three aspect ratios (where AR is defined as the ratio of span to average chord) of 1, 5 and 10 are investigated. Then keeping the same AR, the analysis is repeated for each of the turbines introduced in the preceding sections. The density of the shell, consisting of fiber and glass, is assumed to be 1700 kg/m^3. Table III shows the test cases used for blade shell throw simulations.

Throw distances for the four different turbine sizes with the same working conditions as those for the full-blade case are plotted in Figures 10–12. Here, the non-dimensional length is replaced by the aspect ratio of the blade shell and three different aspect ratios are considered. As can be seen, increasing the hub-height wind speed and the turbine size generally results in larger throw distance. Nevertheless, an erratic behavior, as mentioned in the previous section, appears in the

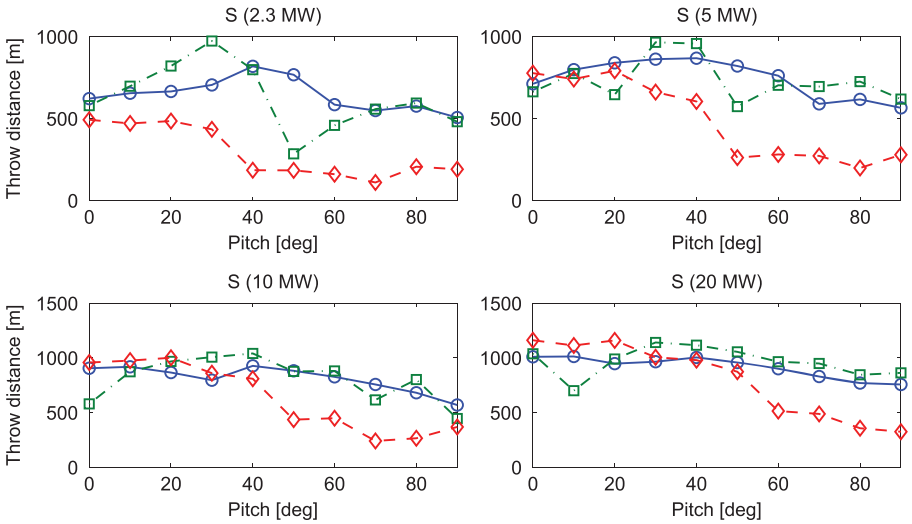

Figure 14. Sensitivity of throw distances of blade shell to the initial pitch setting at V_{tip} = 100 m/s. Legends are the same as in Figure 10.

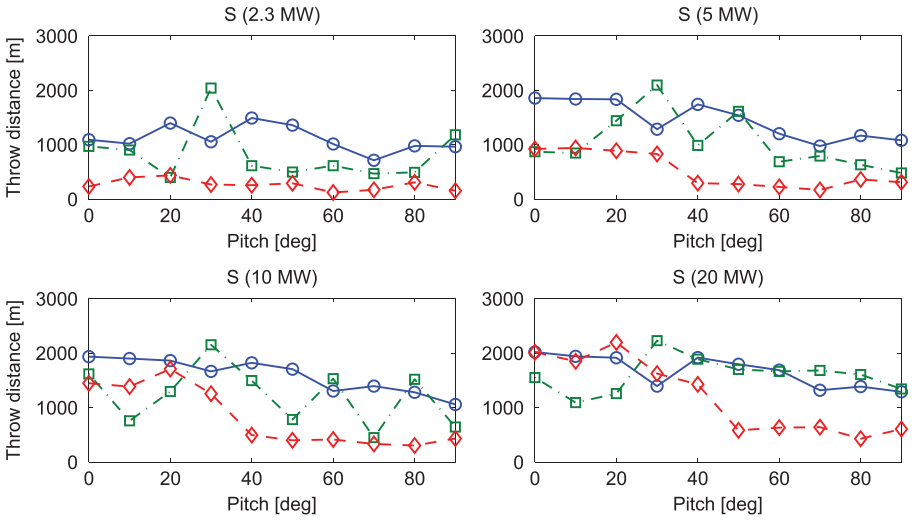

Figure 15. Sensitivity of throw distances of blade shell to the initial pitch setting at V_{tip} = 150 m/s. Legends are the same as in Figure 10.

Wind Energ. 2016; **19**:151–166 © 2015 John Wiley & Sons, Ltd.
DOI: 10.1002/we

simulation results. By comparing the shell-throw graphs with the corresponding figures from the full-blade analysis, the throwing range of the blade shells and that of the full-blade structure are seen to be of the same order of magnitude. That is, the range is between 300 m for the 2.3 MW turbine operating at $V_{tip} = 70$ m/s and a maximum of 2200 m obtained for the 20 MW turbine in the extreme case of $V_{tip} = 150$ m/s. However, unlike the full-blade throw cases, the case with the smallest length ($AR = 1$) reaches the least throw distance, whereas for the full blade, the smallest fragment reaches the highest distance. This is most probably due to the fact that the small shell object is lighter and the corresponding inertial force is relatively small as compared with the drag forces.

As a comparison, the throw distances obtained for the ballistic motion of an equivalent particle in vacuum was also performed (results not shown), in which case there is no aerodynamic forcing on the objects. The results revealed that the ballistic throw distances are the most extreme cases in terms of throw distance.

3.3.1. Effect of initial pitch settings.

Similar to Section 3.2.1, the role of initial pitch setting on the trajectory of thrown blade-shell debris is assessed. Figures 13–15 show the pitch angle dependence of the throw distances for different turbine sizes and tip speeds for the blade-shell cases. Similar to the full-blade throw cases, the pitch setting has a substantial impact on the throw distance of thrown blade-shell structures. One major difference with the full-blade cases is, however, that the effect of the shell aspect ratios on the throw distance is much less significant and all of the cases show similar behavior with AR = 1 cases (red diamonds), predicting smaller throw distances in general.

3.4. Ice throw

For the analysis of the ice throw, the same procedure as for the blade throw is applied except that the throw analysis is not performed for the extreme tip speed conditions but only for the standstill where the tip speed is zero, and the running conditions, where the turbine is assumed to rotate in its normal operational mode at a tip speed of 70 m/s. For the icing case,

Table IV. Aspect ratios, reference chord length C_{ref} and detached mass m of the ice fragments ($\rho_{ice} = 0.7$ kg/m^3) used for throw simulation of turbines of different sizes.

	2.3 MW		5 MW		10 MW		20 MW	
Cases − AR	C_{ref} (m)	m (kg)	C_{ref} (m)	m (kg)	C_{ref} (m)	m (kg)	C_{ref} (m)	m (kg)
$AR = 1$		0.18		0.43		0.97		2.16
$AR = 2$	0.1	0.36	0.15	0.87	0.2	1.95	0.3	4.33
$AR = 3$		0.54		1.31		2.94		6.49

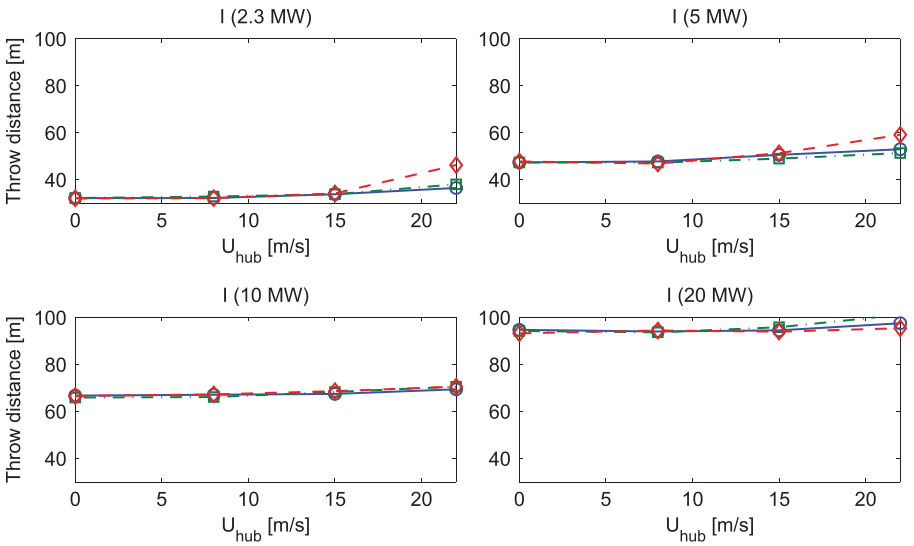

Figure 16. Throw distance calculations of ice fragments for three different aspect ratios for 2.3, 5, 10 and 20 MW turbines in standstill operation ($V_{tip} = 0$ m/s). ◇ ◇ ◇: $AR = 1$; □ □ □: $AR = 2$; and o o o: $AR = 3$.

a density of 700 kg/m^3 is used (see also Seifert *et al.*[11]). The dimensions of the tested ice fragments and corresponding turbine sizes are shown in Table IV. According to field studies performed by, e.g., Cattin *et al.*,[22] most of the ice fragments thrown away from turbine are broken into objects that typically are smaller than 1 kg. However, fragments as heavy as up to 1.8 kg have also been observed. Because the pieces are so light, the throw distance of an ice piece is mainly governed by the drag forces applied on it (which are only functions of mass–area ratio) and the incoming wind.

Similar to the previous section, studies of the effects of different parameters on throw distances are performed and plotted in Figures 16 and 17 with the graphs structured in the same way as in the previous sections.

For the simulations, no lift is considered and the drag coefficient according to the flat-plate assumption is used. Figure 16 shows that the throw distances of the standstill case range from 30 to 100 m for different turbine sizes and incoming wind speeds. For the running conditions however, the fragments can reach distances up to 600 m. It is also clear from the figure that in many cases the aspect ratio does not play a significant role in the determination of throw distances.

3.5. Maximum throw distances

This section presents a summary of the previous results in terms of maximum throw distances. The maximum throw distances are obtained from the entire set of previous simulations regardless of the size and upcoming wind speed and plotted in Figure 18 for the full-blade and blade-shell cases and in Figure 19 for the ice-throw cases, respectively. In all

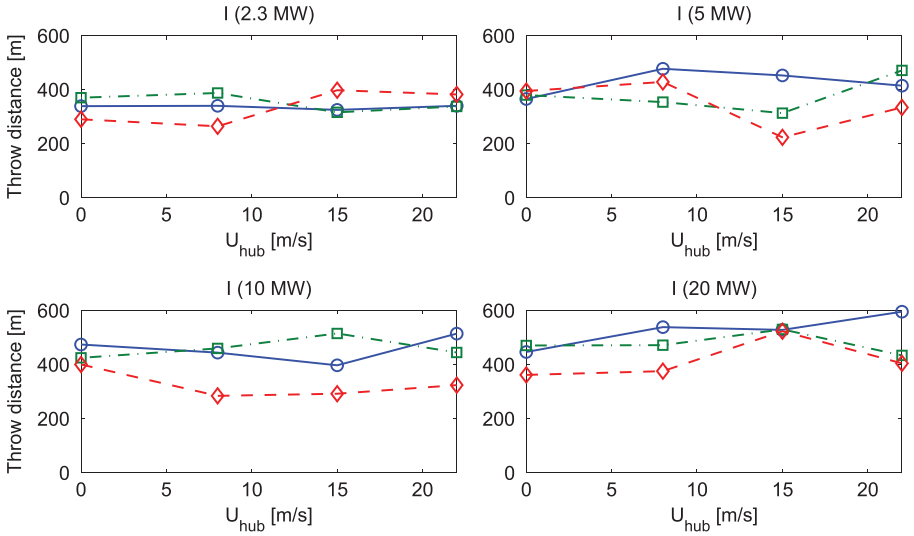

Figure 17. Throw distance calculations of ice fragments for three different aspect ratios for turbines in normal operation (V_{tip} = 70 m/s). Legends are the same as in Figure 16.

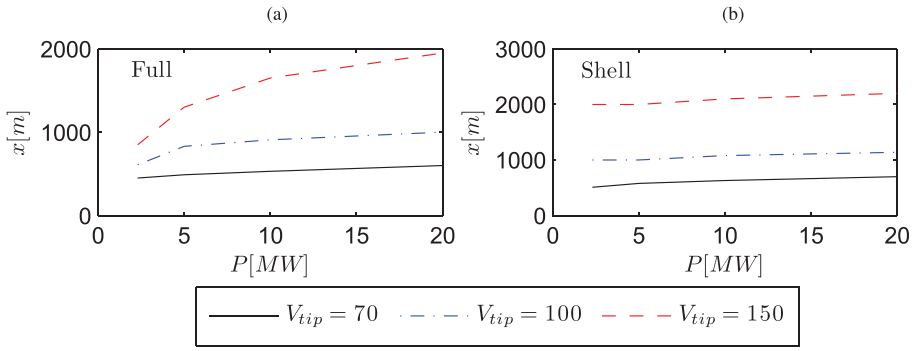

Figure 18. Maximum throw distances obtained for (a) full blade and (b) blade shell in different operating conditions. Blue line: V_{tip} = 70 m/s as a function of turbines power.

Wind Energ. 2016; **19**:151–166 © 2015 John Wiley & Sons, Ltd.
DOI: 10.1002/we

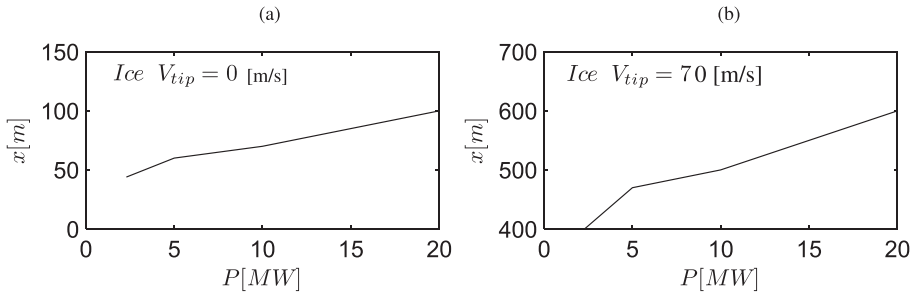

Figure 19. Maximum throw distances obtained for the ice throw in (a) standstill operation, i.e., $V_{tip} = 0$ m/s and (b) normal operating condition, i.e., $V_{tip} = 70$ m/s as a function of turbines power.

figures, the horizontal axis shows the turbine capacity and the vertical axis represents the maximum throw distance. It can be concluded that, in general, the tip speed has a large impact on the throw distances. From Figure 18(a), the turbine size does not affect the throw distances drastically for the lower tip speeds, whereas throw distances at high tip speeds experience a significant growth with increasing turbine size. Figure 18(b), on the other hand, shows that the effect of turbine size on the throw distance for the shell parts is almost negligible.

4. CONCLUDING REMARKS

Trajectory analysis of detached parts of blades and ice fragments thrown from horizontal-axis wind turbines was studied extensively using Newton's and Euler's equations of motion and rotation, employing a blade element approach for the aerodynamics. Full-blade and blade-shell analyses were performed for turbines running under different tip velocities. Turbine upscaling laws were derived, and simulations of throw distances were performed for four different turbine sizes, ranging from existing 2.3 MW machines to future 20 MW turbines.

In some cases, erratic behavior was observed in the computations, where a small change in one parameter could influence throw distance drastically. The behavior was believed to depend highly on the initial conditions. A likely explanation is that a small change in positioning and velocity components in some cases alters the distribution of forces on the detached objects and causes significant changes in the trajectory.

Maximum throw distances obtained at different tip speeds and detachment sizes were analyzed, and it was shown that the tip speed plays the most important role in the throw distance. From the full-blade throw analysis, it was shown that, when released at extreme tip speeds, throw distance picks up more rapidly with the tip speed rather than throw at lower tip speeds (looking at the absolute throw distances). The considered [thrown] full-blade pieces reached approximately 700, 900 and 2000 m at tip speeds of 70, 100 and 150 m/s, respectively. For the blade shell, throw distances were found to be approximately constant as turbine size escalates, and of the same order of magnitude as in the full-blade throw. Throw calculations were also obtained at the tip speeds of $V_{tip} = 0$ and $V_{tip} = 70$ m/s for ice pieces of three different aspect ratios and it was seen that the maximum throw distances scaled almost linearly with the turbine size irrespective of the tip speed. The ice-throw distances reached about 100 and 600 m in standstill $V_{tip} = 0$ m/s and normal operating conditions $V_{tip} = 70$ m/s, respectively. The throw distances presented by this study were obtained with respect to a set of initial parameters without taking into account their probabilities of occurrence. The authors are extending the current study to include the risk levels associated with each of the cases.

REFERENCES

1. Sørensen JN. On the calculation of trajectories for blades detached from horizontal axis wind turbines. *Journal of Wind Engineering* 1984; **8**(3): 160–175.
2. Durstwitz M. *A Statistical Evaluation of Icing Failures in Germany's 250 MW Wind Programme*, BOREAS VI. Pyhatunturi: Finland, 2003.
3. Caithness Windfarms. Summary of Wind Turbine Accident data to 30th September 2012, 2012. Available: http://www.caithnesswindfarms.co.uk/page4.htm, visited Dec 2014.
4. Kirchhoff G. *Mechanik*. Teubner: Leipzig, pp. 232–250, 1897.
5. Aref H, Jones SW. Chaotic motion of a solid through ideal fluid. *Physics of Fluids A* 1993; **5**(12): 3026–3028.
6. Tanabe Y, Kaneko K. Behaviour of falling paper. *Physical Review Letters* 1994; **73**(10): 1372–1375.

7. Pesavento U, Jane Wang Z. Falling paper: Navier-Stokes solutions, model of fluid forces and center of mass elevation. *Physical Review Letters* 2004; **93**(14): 144501–1:4.
8. Andersen A, Pesavento U, Jane Wang Z. Unsteady aerodynamics of fluttering and tumbling plates. *Journal of Fluid Mechanics* 2005; **541**: 65–90.
9. Macqueen JF, Ainsilie JF, Milborrow DJ, Turner DM, Swift-hook DT. Risks associated with wind-turbine blade failures. *IEEE Proceedings-Part A* 1983; **130**(9): 574–586.
10. Rogers J, Slegers N, Costello M. A method for defining wind turbine setback standards. *Journal of Wind Energy* 2012; **15**(2): 289–303.
11. Seifert H, Westerhellweg A, Kroning J. Risk analysis of ice-throw from wind turbines. *Proceedings BOREAS 6*, Pyha, Finland, 2003; 1–9.
12. Biswas S, Taylor P, Salmon J. A model of ice-throw trajectories from wind turbines. *Journal of Wind Energy* 2012; **15**(7): 889–901.
13. Morgan C, Bossanyi E, Seifert H. Assessment of safety risks arising from wind turbine icing. *Proceedings of BOREAS IV Conference*, Hetta, Finland, 1998; 113–121.
14. Morgan CA, Bossanyi EA. Wind turbine icing and public safety – a quantifiable risk. *Proceedings of BOREAS III Conference*, Sariselka,Finland, 1996; 141–144.
15. Sørensen J. Prediction of site risk levels associated with failures of wind turbine blades. In *European Wind Energy Conference*. H.S. Stephens & Associates: Bedford, England, 1984; 344–349.
16. Carbone G, Afferrante L. A novel probabilistic approach to assess the blade throw hazard of wind turbines. *Renewable Energy* 2013; **51**: 474–481.
17. Ragheb M. Safety of wind systems. Available: http://www.windfarmaction.files.wordpress.com/2011/10/safety-of-wind-systems.pdf [accessed on Dec 2014].
18. Øye S. Dynamic stall simulated as time lag of separation. In *Proceedings of the Fourth IEA Symposium on the Aerodynamics of Wind Turbines*, K McAnulty (ed.). ETSU, Harwell, 1991; 6.1–.7.
19. Wyngaard J. *Turbulence in the Atmosphere,* (1st ed). Cambridge University Press: Cambridge, UK, 2010.
20. UpWind, Design limits and solutions for very large wind turbines. *European Wind Energy Association (EWEA) Technical Report*, Brussels, Belgium, 2011. Available: www.ewea.org [Accessed on Dec 2014].
21. Parametric study for large wind turbine blades. *Sand2002-2519 Report*, Sandia National Laboratories USA, 2002.
22. Cattin R, Kunz S, Heimo A, Russi G, Russi M, Tiefgraber M. Wind turbine ice-throw studies in the Swiss Alps. *Proceedings of the EWEC Conference*, Milan, Italy, 2007; 1–5.

Wind Energ. 2016; **19**:151–166 © 2015 John Wiley & Sons, Ltd.
DOI: 10.1002/we